

Ozone decrease observed in the upper atmosphere following the May 11th 2024 Mother's Day ~~and the June 8th solar storm~~ storms.

Alexandre Winant^{1, 2}, Viviane Pierrard^{1, 2}, and Edith Botek¹

¹Solar Wind, Space Physics and Solar-Terrestrial Center of Excellence, Royal Belgian Institute for Space Aeronomy (BIRA-IASB), Avenue Circulaire 3, Brussels, Belgium

²Earth and Life Institute, Climate Sciences ELI-C, Université Catholique de Louvain (UCLouvain), Louvain-la-Neuve, Belgium

Correspondence: Alexandre Winant (alexandre.winant@aeronomie.be)

Abstract. On May 11th 2024, a succession of coronal mass ejections that merged together struck the Earth and induced large-scale perturbations in the magnetosphere. During this event, satellite observations showed a large solar ~~energetic proton (SEP) event~~ proton event (SPE) associated to an extreme geomagnetic storm. At the same time, satellite observations of atmospheric ozone ~~have been performed by~~ and temperature were performed by the AURA/MLS instrument. In this work, we present 5 the first observations of the effect of the storm of May and the following ~~SEP~~ SPE of June 8th on ozone concentration and temperature throughout the atmosphere. Observations of the MLS instrument show that the event of May led to stronger depletion of ~~O₃ in the upper part of the atmosphere~~ O₃ in the mesosphere and lower thermosphere (MLT) than in June and that noticeable depletion mainly occurred in the southern hemisphere. This difference is explained by the type of particle precipitation that occurred during the two events, with both protons and electrons in May and only protons in June. ~~Neither~~ 10 Although both SPEs caused an increase of the ionization rates down to 30 km, neither event caused ozone depletion in the stratosphere ~~while strong decreases are observed in the mesosphere. In~~ Above 85 km, a decrease of ozone volume mixing ratio (vmr) was observed together with an increase of the temperature following the event of May while no changes in ozone is observed following the SPE of June. Finally, in May, mesospheric ozone depletion ~~is observed during 18 days and~~ reaches a maximum of 60% ~~. In addition, the storm of May at 80 km lasting for 18 days and 30% at 75 km lasting for 5 days. The SPE~~ 15 of June also caused a ~~noticeable decrease in ozone concentration (up to 20%) at altitudes above 90~~ decrease of mesospheric ozone that lasted for 3 days down to 70 km.

1 Introduction

While solar cycle 25 is approaching its maximum activity (~~predicted in 2025~~ (Pesnell and Schatten (2018))), the probability of strong solar events is also expected to rise. Both the frequency and the intensity of solar events increase around the maximum and the declining phase of the cycle. ~~The year 2024 is located at the end of the ascending phase of cycle 25, making it prone to be subjected to large perturbations of solar origin, although the strongest events take generally place during the descending phase (Abe et al. (2023)).~~ On the 11th of May 2024, an extreme geomagnetic storm associated with a large Forbush ~~decrease~~ 20 decrease in galactic cosmic rays were observed on the ground ~~Mavromichalaki et al. (2024)~~ (Mavromichalaki et al. (2024)).

The cause of the extreme event of May 2024 ~~is was~~ a succession of ~~CMEs (Coronal Mass Ejections~~coronal mass ejections
25 ~~(CMEs)~~ that merged together and simultaneously struck the Earth, which ~~lead led~~ to an extreme perturbation of the magne-
tosphere ~~Kwak et al. (2024). Moreover, a large Solar Energetic Particle (SEP) event was observed (Kwak et al. (2024)). The~~
~~CMEs were associated to a large solar proton event (SPE) that was observed on May 10th in the vicinity of the Earth by space~~
~~borne particle detectors Pierrard et al. (2024). This geomagnetic storm is~~spaceborne particle detectors (Pierrard et al. (2024)
). ~~The geomagnetic storm was~~ the largest observed in more than 20 years, reaching a minimum ~~Disturbed-Disturbance~~
30 ~~Storm time index $Dst_{min} = -412$ $Dst_{min} = -412$ nT and a maximum Bartels planetary index of geomagnetic activity~~
 ~~$Kp_{max} = 9$ $Kp_{max} = 9$~~ . The last observation of an event with a similar magnitude dates back to the famous 2003 Halloween geo-
magnetic storm with a minimum ~~Dst_{min} around -400 nT.~~ Dst_{min} around -400 nT. A recent study by Elvidge and Themens (2025)
shows that this storm was a 1 in 12.5 year event in term of magnitude and a 1 in 41 year event in term of duration. Moreover, this
event was categorized as the sixth strongest storm observed since 1957 (Hayakawa et al. (2025)). The geomagnetic storm of
35 May 11th was responsible for large variations in the ~~radiation belts of the Earth, in which~~terrestrial radiation belts, where a tem-
porary 4 belts structure was observed at low Earth orbit ~~Pierrard et al. (2024). On the 8th of June 2024, 27 days after the extreme~~
~~event of May, another SEP event has been observed near Earth. (Pierrard et al. (2024)). Observations of major disturbances in~~
~~the ionosphere have also been reported all over the globe (Themens et al. (2024); Singh et al. (2024); Huang et al. (2024); Pierrard et al. (20~~
~~)~~. ~~In addition, enhanced Joule heating caused by the storm of May led to a sharp rise in the thermospheric densities due to~~
40 ~~cooling from increased NO concentration (Ranjan et al. (2024)). At lower altitudes in the thermosphere, measurements from~~
~~the GOLD instrument showed global changes in composition and temperature following the event, with temperature increasing~~
~~up to 1400 K at high latitudes at 160 km (Evans et al. (2024)). Global increase of temperature in the mesosphere and lower~~
~~thermosphere was also reported by Liu et al. (2025).~~

Enhanced geomagnetic activity also leads to increased energetic electron precipitation (EEP) in the atmosphere at high lat-
45 ~~itudes, which.~~ They mainly consist of auroral electrons originating from the magnetotail and radiation belt electrons in the
bounce loss cone. Energetic protons of solar origin also precipitate in the atmosphere as they are guided toward high latitudes
by the Earth's magnetic field. As they penetrate into the atmosphere, energetic particles interact with the constituents of the at-
mosphere inducing ~~their~~ excitation, dissociation and ionization ~~Sinnhuber et al. (2012); Mironova et al. (2015). Following the~~
~~interaction of the atmosphere with the energetic precipitating particles (EPP), complex chains of chemical reactions take place~~
50 ~~in different layers of the atmosphere, which can lead to the formation of odd hydrogen ($HO_x = H + HO + HO_2$) and odd~~
~~nitrogen ($NO_x = N + NO + NO_2$) via ion-neutral chemistry Verronen and Lehmann (2013). NO_x (Sinnhuber et al. (2012); Mironova et~~
~~)~~. Subsequent neutral-ion chemistry leads to the formation of odd hydrogen ($HO_x = H + HO + HO_2$) and odd nitrogen ($NO_x = N + NO + N$
(Solomon et al. (1981, 1982); Turunen et al. (2009); Rozanov et al. (2012); Verronen and Lehmann (2013)). Increased HO_x productions
by SPE mainly occur in the mesosphere and upper stratosphere and is expected to efficiently destroy ozone through a well-known
55 ~~chain of catalytic reactions (Verronen et al. (2006); Grenfell et al. (2006)). In addition to SPE, EEP from the radiation belts~~
~~have been found to also have a significant influence on HO_x production in the mesosphere (Verronen et al. (2011); Andersson et al. (2012)~~
~~)~~. At these altitudes, HO_x has a short lifetime of a few hours (Pickett et al. (2006)) and its impact on ozone is fast but
also of short duration (a few days) (Smith et al. (2018b)). During the SPE events of January 2005 and December 2006,

60 both satellite observations and simulations have shown a temporary destruction of mesospheric ozone caused by boosted concentration of HO_x (Verronen et al. (2006); Seppälä et al. (2006); Sofieva et al. (2009)). Similarly, EEP can be responsible for ozone depletion between 60 km and 80 km by 90% on short time scales (Andersson et al. (2014)). Nitrogen oxides NO_x are mainly produced in the upper part of the atmosphere, in the mesosphere (50 to 90 km) and lower thermosphere in the lower thermosphere (90 to 100 km), where their production rate concentration is increased by EPP Sætre et al. (2004). These species have a long atmospheric lifetime, especially during the polar winter. In the presence of the polar vortex, NO_x produced in the mesosphere and lower thermosphere (MLT) region can be efficiently transported downward (SPE + EEP) (Sætre et al. (2004); Turunen et al. (2009)). Odd nitrogen is long lived in the atmosphere at those altitudes in the absence of Sun light. During polar winter, NO_x can be accumulated and transported downward without significant losses to the stratosphere (10 to 50 km in average) and deplete the ozone in this region of the atmosphere Randall et al. (2007); Funke et al. (2014, 2016). Mesospheric HO_x levels have been observed to correlate with the precipitation of electrons from the radiation belts Verronen et al. (2011); HO_x are short lived, thus their response to EPP is localized in space and time, where and when ionization is increased Mironova et al. (2015). HO_x and NO_x contribute to the depletion of ozone by the Brewer–Dobson circulation inside the polar vortex (Funke et al. (2005)) and efficiently deplete ozone through catalytic reactions Lary (1997). Thus, the net result of EPP is to contribute to decrease the ozone concentration in the atmosphere and can have repercussion on climate Rozanov et al. (2012); Seppälä et al. (2012).

75 The response of ozone in the atmosphere to EPP (of both protons and electrons) has been extensively studied over the years. Energetic Electron Precipitations (EEP) have been found to have a significant influence on O_3 in the mesosphere between 60 km and 80 km, where it could be depleted by 90% on a short term scale Andersson et al. (2012); (Lary (1997); Jackman et al. (2001); Randall et al. (2007)). Because they have the possibility to ionize lower layers in the atmosphere, energetic solar protons may can contribute to deplete ozone in the upper stratosphere. However, strong evidence of stratospheric ozone depletion associated with SEP are scarce SPE is rare because of the rarity of extreme SPEs. In the study of Jia et al. (2020), changes of ozone were observed by MLS after SEPs MLS observed ozone variations after SPEs between 2004 up to and 2020. Although clear ozone depletion can be observed at high altitudes following multiple SEPs SPEs, only one event was found to have an effect on the stratospheric ozone in 2005. Moreover, Funke et al. (2011) reported that upper stratospheric ozone was directly depleted following the extreme SPE that accompanied the 2003 'Halloween' superstorm.

85 In this paper, we use observations from the Microwave Limb Sounder (MLS) to investigate and provide a first report of the effect of the extreme solar and geomagnetic event of May as well as the following SEP SPE of June on atmospheric ozone in the polar regions.

2 Data and methods

2.1 Ozone and temperature observations from AURA/MLS

90 The Microwave Limb Sounder (MLS) as part of the Earth Observing System (EOS) Evans and Greer (2000) (Evans and Greer (2000)) was launched in 2004 onboard the NASA satellite AURA on in quasi-polar sun-synchronous Sun-synchronous orbit at 705

km of altitude. This instrument measures thermal radiation from Earth's atmosphere by retrieving vertical profiles of the temperature and trace gases, by scanning Earth's limb in the plane of its orbit. In this work, we mainly use ~~ozone profiles from the MLS-MLS ozone profiles~~ that are derived from ~~radiancees-radiance~~ measured by the 240 GHz radiometer. More specifically, we use the latest version v5.0 of the MLS data product with a spatial coverage ranging from -82° to 82° and that has an increased vertical range compared to previous versions (Schwartz (2021)). ~~The vertical resolution is not constant with altitude, it is around 2 km between 25 km and 50 km, around 3 km between 50 km and 65 km and around 4.5 km between 65 km and 93 km. With v5.0, ozone observations in the upper mesosphere are available for scientific studies.~~ In this work, we have applied all recommendations regarding data screening provided in the *MLS Level 2 Version 5 Quality Document* that can be found at (https://mls.jpl.nasa.gov/data/v5-0_data_quality_document.pdf). Moreover, we only ~~use high latitude observations, used high-latitude observations~~ comprised between 60° and ~~90~~ 82° in both hemispheres ~~and then perform, and then performed~~ daily averages which are necessary for the highest altitudes in the mesosphere ~~-(Level and lower thermosphere. (MLS level 2 ozone data from MLS~~ are available at https://disc.gsfc.nasa.gov/datasets/ML2O3_005/summary, last accessed on 29/10/2024).

105 2.2 In situ observations of energetic particles

For the solar proton fluxes, we use ~~the~~ observations from the Geostationary Operational Environmental Satellite (GOES) which is fitted with the Energetic Proton, Electron, and Alpha Detector (EPEAD). This instrument measures the flux of protons in 7 energy channels spanning from 0.74 to 900 MeV. The data used in this work ~~consists-consist~~ of integral proton fluxes with energies > 10 MeV, > 30 MeV, > 100 MeV which have a resolution of 5 minutes. (Data are accessible at: <https://lasp.colorado.edu/space-weather-portal/>, last accessed on 29/10/2024).

In order to determine when energetic electrons from the radiation belts precipitate into the atmosphere, we ~~use-used~~ the POES/MEPED detector on the MetOP satellite. The MEPED instrument is composed of two pairs of directional detectors. The first pair is dedicated to the measurement of protons with energies ranging from 30 keV to 200 MeV. The second pair of detectors measures the fluxes of electrons of energies between 30 keV to 2500 keV in 3 integral channels. For a given type of particles, the two telescopes are arranged perpendicular to one another and are referred to as the 0° telescope and the 90° telescope. On ~~MetOp~~MEPED, the 0° telescope points directly to the zenith, and the 90° telescope points to the antiram direction (i.e., opposite to the velocity vector of the spacecraft). At high latitudes, the 0° telescope mainly measures particles in the Bounce Loss Cone (BLC) and thus precipitating into the atmosphere.

2.3 Computation of the ionization rates

120 To compute the ionization rate in the atmosphere induced by energetic solar protons, we use the GEANT-4 based Atmospheric Radiation Interaction Simulator (AtRIS) developed by Banjac et al. (2019). The atmospheric parameters for the simulation are computed with the NRLMSISE model as in Winant et al. (2023) and are set to 90° S in May 2024. In this run, the primary particles are Galactic Cosmic Ray (GCR) and solar protons. The spectrum of GCR is computed with the solution of the force-field approximation and the Local Interstellar Spectrum (LIS) proposed by Herbst et al. (2017). For solar protons, the

125 [daily differential spectra observed by GOES are fitted with the Ellison and Ramaty parameterization \(Ellison and Ramaty \(1985\)](#)

[\)](#)

2.4 Assessing the impact on ozone and temperature

The ~~main strategy~~ [first approach](#) to quantify the effect of the May and June events on ozone through the atmosphere is taking the average profile of ozone before the event (quiet ozone profile), and computing its difference relative to the daily profiles
130 for the rest of the month. The quiet period consists of the five daily profiles observed before either the maximum proton flux observed by GOES or the minimum in the Dst index. Those profiles are then averaged on time to provide the quiet conditions.

~~Another~~ [The second](#) approach used in this work is to first compute the ~~long-term~~ [long-term](#) trend in the profiles observed by MLS. In order to do so, a lowess (locally weighted ~~scatterplot~~ [scatter plot](#) smoothing) algorithm, [introduced by Cleveland \(1979\)](#) was applied to the daily profiles from MLS spanning from January 1st 2024 to June 30th [2024](#). [In practice,](#)
135 [we use the lowess function from the Statsmodel python library with a value of frac = 0.25](#). With the results of the lowess algorithm, the daily detrended profiles are computed, revealing only the ~~short-term~~ [short-term](#) variations which can then be compared to daily averaged geomagnetic activity.

3 Results

3.1 [AURA/MLS ozone profiles](#)

140 Figure 1 shows the daily averaged MLS ozone profiles at high latitudes from the beginning of 2024 to June 30th. The top panel corresponds to the high southern latitudes comprised between -60° and ~~-90.82°~~ [of latitude](#) and the middle panel corresponds to the northern latitudes comprised between 60° and ~~90.82°~~ . The bottom panel of this figure shows the geomagnetic activity for the period, displaying both the Dst and Kp indices. They indicate that during the beginning of the year, the geomagnetic activity is very low, with the Kp index barely exceeding 4. It is only in March that a noticeable geomagnetic storm was recorded in both
145 Dst and Kp. The next big event took place in ~~mid-April~~ [mid-April](#) with a Dst below -100 nT and a Kp of 7. ~~Form~~ [From](#) this point onward, these indices show that the magnetosphere was repeatedly disrupted by intense storms until the extreme event of May 11 occurred with a minimum Dst value never seen in 20 years of -412 nT and a Kp of 9. During the recovery phase of this major event, some other intense events took place ~~and~~. [Later](#), the Dst index remained quiet until the end of June.

~~All along~~ [Throughout](#) this period, the AURA/MLS instrument continuously carried out measurements of ozone throughout
150 the atmosphere. The first panel of Fig. 1 clearly illustrates the different ozone layers that exist in the atmosphere. The main ozone layer located in the stratosphere ([below 50 km](#)), the secondary layer in the upper mesosphere and lower thermosphere (MLT) region ([above 85 km](#)) and finally the tertiary layer in the mesosphere where the maximum of ozone concentration is observed at around 75 km. Both the second and third ozone layers are subjected to very strong seasonal variations and are mostly depleted during local summer due to increased photodissociation ([Marsh et al. \(2001\); Smith and Marsh \(2005\); Smith et al. \(2018a\)](#)).

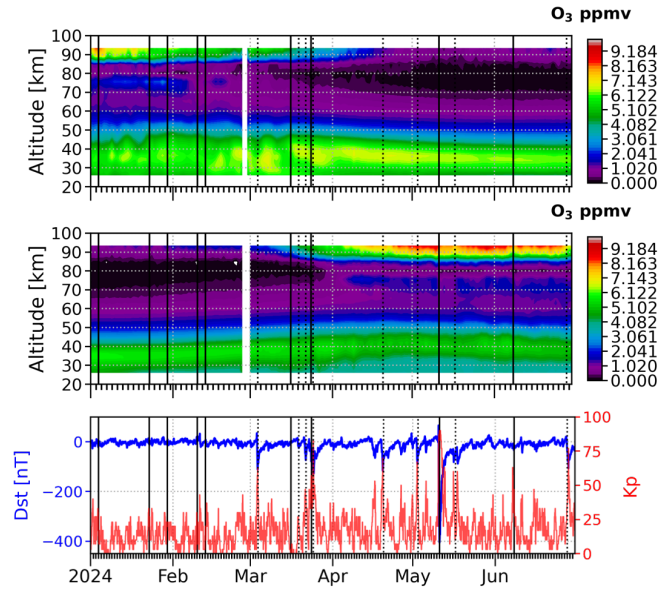


Figure 1. Daily averaged high latitude ($[60^{\circ}, 90^{\circ}]$) ozone volume mixing ratio profiles from AURA/MLS as a function of time and altitude between January 1st and June 30th 2024. Top: northern hemisphere. Middle: southern hemisphere. Ozone volume mixing ratio is expressed in parts per million by volume (ppmv). Bottom: Geomagnetic activity indices from the OMNI database between January 1st and June 30th 2024. The Disturbed-Disturbance storm time (Dst) index is represented in blue and the planetary Kp index multiplied by 10 is displayed in red. The vertical dotted lines correspond to geomagnetic storms with $Dst < -50$ nT and the plain lines correspond to SPE events for which the flux of protons with > 10 MeV have exceeded $10 p / (cm^2 s sr)$.

Thus in the northern hemisphere (NH), the ozone forming present in the secondary and tertiary layers gradually gets depleted-diminishes from winter to summer, when the During this period, mesospheric ozone is completely-almost entirely removed from the atmosphere and the secondary layer ozone, decreasing from approximately 2.5 ppmv to below 1 ppmv, while the ozone in the secondary layer is reduced from between 7 and 8 ppmv to between 1 and 2 ppmv. In the southern hemisphere (SH) (middle panel of Fig. 1), the situation is reversed and ozone starts to accumulate in the mesosphere and the lower thermosphere.

In addition to the strong seasonal variations of ozone, the first and second panel-panels of the figure clearly show that the ozone also experiences short-term variations. Those variations on smaller time scales are not linked short-term variations. The vertical lines on the figure correspond to geomagnetic storms illustrated by high peaks of geomagnetic activity in the bottom panel, in any of the ozone layers.

In order to observe a direct effect of solar energetic particles (SEP) in the stratospheric ozone layer, there must be a significant flux of protons with sufficient energy to ionize the stratosphere. Between January and May, some minor SEP events did occur but they had low fluxes and a soft spectrum which could not have impacted the stratospheric ozone. Soft protons can deposit

170 their energy in the mesosphere, and some rapid decreases in O_3 happened in the NH after the particles injections at high altitudes, but not always. After the May 11 events, no ozone is left (dotted lines when not associated to SPEs) and SPEs (solid lines) that occurred between January and June 2024. In the NH, at the beginning of the year, when ozone is present in the upper part of the atmosphere so that no ozone is lost further. Despite their hard spectrum and high fluxes, neither the May nor the June SEPs (see Fig. 2) have had any impact on the NH main ozone layer. One of the reasons might be due to atmosphere, the weakening of the polar vortex in the NH during late spring and summer.

175 short-term variability observed in those layers is not clearly linked to either the observed SPEs, nor to geomagnetic activity. In the SH, in the beginning of the year, no ~~short term variation of O_3 has been observed by MLS.~~ short-term variation of O_3 observed by the MLS instrument appears to be related to geomagnetic activity nor to SPEs. This is mainly due to the fact that only very small amounts of ozone are present above 60 km until the end of March. However, the middle panel of Fig. 1 clearly shows a change ~~of in~~ ozone concentration in the ~~MLT~~ lower thermosphere region (at ~ 90 km), as well as in the mesosphere

180 (at ~ 75 km) after the event of May. In the stratosphere, no sign of the event of May is discernible in the figure. In the NH, no significant variations of ozone can be seen in the figure following the events of May and June in any of the ozone layers.

3.2 Precipitating particle fluxes measured by GOES and POES

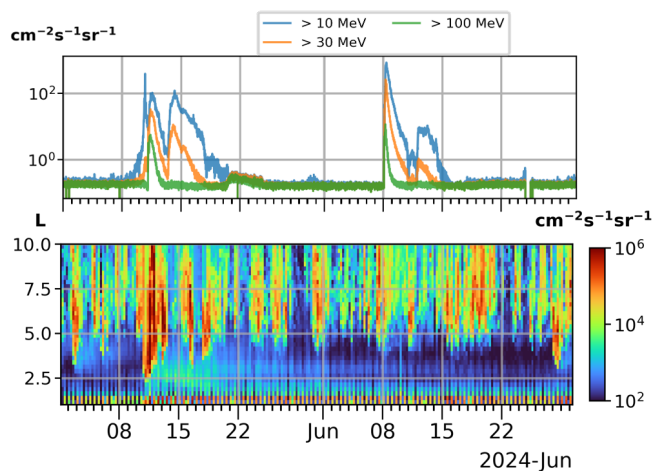


Figure 2. Top: Integral proton flux measured by GOES between May 01 and June 30, 2024 in three different energy channels. Bottom: Integral electron flux with energy >30 keV measured by POES 0° telescope and averaged in L-time bins [0.1L - 3h] displayed as a function of time and the McIlwain L parameter over the same time period.

The ~~flux of EPP fluxes of energetic precipitating particles (both protons and electrons)~~ between May 1st and June 30th 2024 are presented ~~on the two in both~~ panels of Fig. 2. On the top, GOES observations of the integral proton fluxes with different energy threshold clearly show the two ~~SEP-SPE~~ events of May 11th and June 8th. This panel reveals that each of the two ~~SEPs~~ have a double peak in protons of >10 MeV and >30 MeV but not for protons with energies >100 MeV. ~~SPEs generates~~

185

multiple peaks for protons of > 10 MeV and > 30 MeV due to repeated injections, wave-driven acceleration and relatively slow loss processes. In contrast, a single peak is observed for > 100 MeV fluxes. The proton flux measured by GOES in June is very similar to the flux of May (see Fig. 2 top panel), because they originate from the same region. Both SPEs were likely produced by the same active region at the surface of the Sun and they are separated in time by one solar rotation that was still active after one period of rotation (Jaswal et al. (2025)).

The second panel of Fig. 2 displays the integral flux of electrons with energies > 30 keV observed by the MEPED 0° telescope during the same period as GOES. In this case, the electron fluxes are presented as a function L, the McIlwain parameter (uniquely identifying Earth's magnetic shells) and time. Electron fluxes have been averaged on L-time bins of 0.1 L and 3 hours. At high latitudes and thus high L values, electrons observed by the 0° telescope are considered to precipitate into the atmosphere along the magnetic field lines (Rodger et al. (2010)). Unlike SEP (Rodger et al. (2010)), unlike SPE events, electron precipitation in the atmosphere is a process that is constantly occurring, but it is modulated by geomagnetic activity. Increased precipitation has been observed during the main phase of the geomagnetic storm of May 11 reaching the maximum flux of $\sim 1.2 \cdot 10^6$ [cm²s sr]⁻¹ which is never attained again throughout the whole period.

3.3 Simulations of ionization rate

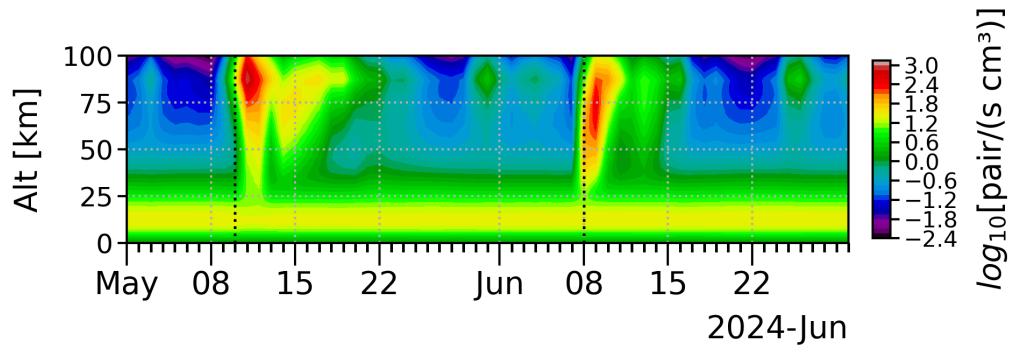


Figure 3. Top panel: The plain lines represent the daily averaged ozone vmr computed with AURA/MLS observations from May 1st and June 30th. Daily ionization rate profiles [in the Southern hemisphere. The dashed lines are the pair/s cm³] computed long-term trends in ozone vmr resulting from the lowess algorithm applied with AtRIS based on the observations from January to June. GOES differential proton flux. Each color corresponds to an altitude level. Bottom panel: The daily detrended ozone vmr. Colors are the same as for the top panel. The vertical black dotted line represents mark the day during which the daily averaged Kp-index multiplied by 10 protons fluxes computed from omni-data GOES observations begin to increase.

Figure 3 shows ionization rates between 0 km and 100 km that result from the AtRIS simulation considering primary GCR and energetic solar protons. The background GCRs, which are the most energetic, are responsible for the ionization maximum at low altitudes (between 10 km and 20 km), known as the Pfozter maximum. The contribution from the less energetic solar

205 protons can be clearly observed on the figure during the two SPEs of May and June. Both events feature a similar temporal evolution with a large initial increase in ionization that reaches 30 km of altitude and lasts for 2 days followed by a smaller increase in ionization that remains at higher altitude (above 40 km). Despite those similarities, the changes in the ionization in the atmosphere during the two events are different. The rise in ionization rates caused by the SPE of May lasted longer and was higher than in June. During the event of May, the peak of ionization is observed at 86 km and reaches 1000 [pair/(s cm³)] whereas the peak of ionization during the event of June is observed at 73 km and reached 280 [pair/(s cm³)]. Following

210 the initial injection of more energetic protons, the second flux peak of solar protons in May caused significantly increased ionization rates (up to 37 [pair/(s cm³)] at 90 km until May 22nd. In June, the second flux peak of solar protons caused the ionization rates to increase up to 10 [pair/(s cm³)] at 90 km until June 16th.

3.4 Detrended ozone profiles in the southern hemisphere

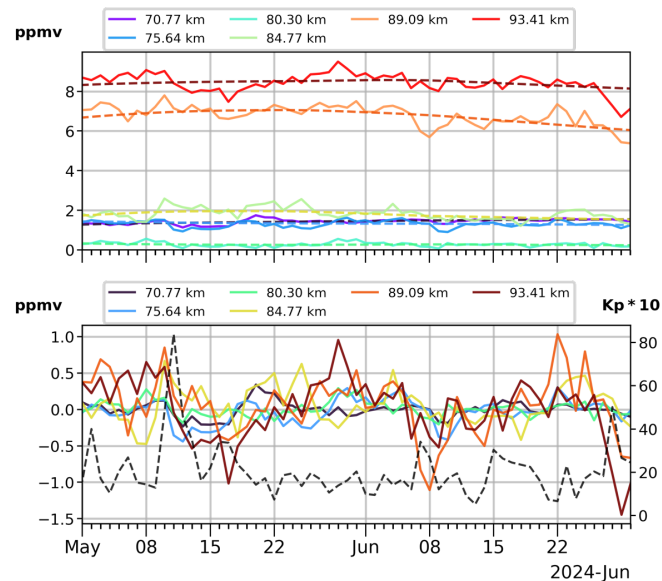


Figure 4. Top panel: The plain lines represent the daily averaged ozone vmr computed with AURA/MLS observations from May 1st to June 30th in the southern hemisphere. The dashed lines are the computed long-term trends in ozone vmr resulting from the lowess algorithm applied on the observations from January to June. Each color corresponds to an altitude level. Bottom panel: The daily detrended ozone vmr. Colors are the same as for the top panel. The black line represents the daily averaged Kp index multiplied by 10 computed from OMNI data.

215 As ozone concentration in the atmosphere is subject to seasonal variations and changes on longer time scales such as the solar cycle, we computed the long-term-long-term variations in the MLS observation-observations in order to extract only the ozone changes on small time scales between May 1st and June 30th. The long-term-long-term trend in MLS observations was computed by applying the lowess algorithm on the daily ozone profiles. To ensure that the results of the algorithm could

capture the seasonal variability, we used the data from January 1st to June 30th to compute the trend. The result of this data treatment is shown in the top panel of Fig. 4 together with the daily average ozone ~~volume mixing ratio (vmr)~~vmr. Each color
220 in the figure represents an altitude level ranging from 70 km to ~~97-93~~93 km, covering the mesosphere and lower thermosphere. The bottom panel of the figure shows the detrended ozone vmr (i.e., daily ozone vmr minus the ~~long-term~~long-term trend) at each altitude level. The black curve in this panel corresponds to the daily averaged Kp index (multiplied by 10) computed from the OMNI dataset. From this panel, it is clear that, following the peak in the Kp index which indicates the main phase of the geomagnetic storm of May 11th, a rapid decrease in ozone vmr is observed by the MLS ~~instrument for all altitudes between 70~~
225 ~~km and 93 km~~ km. It then required 18 days for the ozone vmr to regain the pre-storm levels. In June, no major geomagnetic storm took place as shown by the daily Kp curve. However, the detrended ozone shows a noticeable decrease on the 7th of June at 84 km. At ~~higher-lower~~altitudes, the decrease in ozone occurs on the 9th, after the ~~SEP-event~~SEP event ~~SPE~~ took place.

3.5 Observations of ozone and temperature in May

Figure 5 displays the ~~results of the daily averaged measurements of O₃ (top left) and temperature (top right) in the southern~~
230 ~~polar atmosphere, as well as their~~ relative difference in percentage between the pre-storm (i.e. ~~quiet~~quiet) ozone vmr (top panel), ~~as well as temperature profile (bottom panel), quiet~~ level and all the daily profiles measured from the start of the period until the end of the month. The ~~bottom left panel shows the results for the ozone and the bottom right shows the results for the~~
~~temperature. The~~ quiet period consists of the time averages of the daily profiles between May 5th and May 9th. The reason for not taking the profiles between the 6th and ~~10th-10th~~10th is that, even if the peak of the ~~SEP-SPE~~SEP-SPE flux and the ~~main-phase~~main-phase peak of
235 the geomagnetic storm took place on May 11th, the flux of lower energy protons (> 10 MeV) has a first peak on the 10th of May. So that May 10th is neither considered as a quiet day ~~nor is the~~, ~~as it also corresponds to the beginning of the main phase~~
~~of the geomagnetic storm, even if the~~ peak of the event (when considering the proton spectrum and the geomagnetic activity) ~~appeared at the~~
~~beginning of May 11.~~

240 ~~From the top panel of the figure, it is obvious that some ozone was lost during the period of interest.~~The vertical black dotted line indicates the day during which ~~the daily averaged proton flux and geomagnetic activity are the highest~~solar proton fluxes observed by GOES begin to rise (i.e. May ~~11th~~11th). ~~The~~10th, before reaching their peak on May 11th together with the highest geomagnetic activity for the period. Both left panels of Fig. 5 show that the main ozone loss ~~was observed~~takes place after the event in the tertiary layer at around 75 km. ~~However, the day before, The 20% decrease of ozone in the mesosphere~~
245 ~~began~~ on May 10th, ~~the ozone vmr at those altitudes had already decreased by 20%. This premature decrease might be. This initial decrease was~~ caused by the penetration of ~~the~~low energy protons measured by GOES on that day, which efficiently deposit their energy around 70 km (see Fig. 1 of Satori et al. (2016)). ~~Figure 3 also shows that the ionization rate on May~~
~~10th was already increased in those regions.~~ Two days after the main phase of the storm ~~corresponding to the maximum flux~~of precipitating electrons, ozone vmr at 80 km decreased by as much as 60%. This ozone deficit relative to pre-storm level
250 remained until May 29th, oscillating between 30 % ~~to~~and 50%. ~~However, those values must be taken with caution since this altitude corresponds to the minimum between the tertiary and the secondary ozone layers, and the near-zero values of ozone in~~

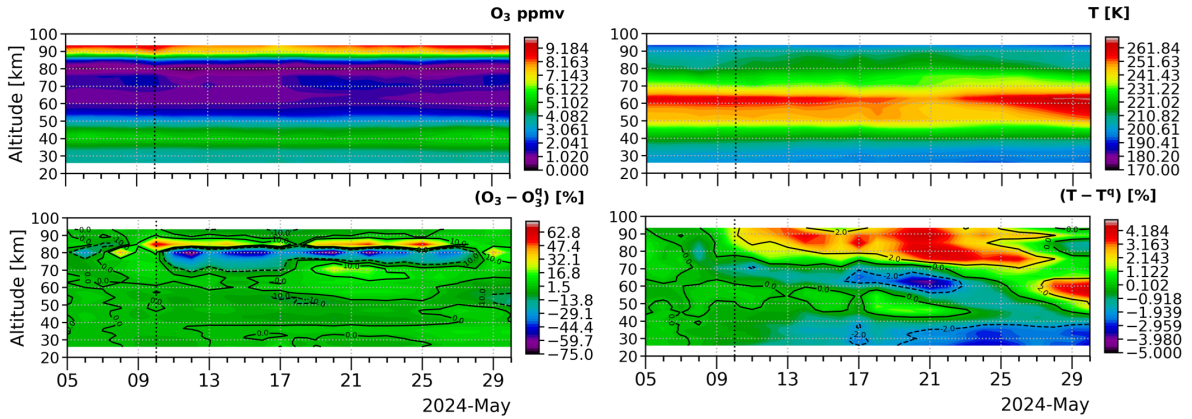


Figure 5. Top left panel: Absolute values of the O_3 vmr measured by the AURA/MLS instrument in the southern hemisphere throughout the month of May 2024. Bottom left panel: Relative difference (in [%]) between the mean quiet condition ozone profiles (O_3^q) and the daily ozone profiles from the AURA/MLS instrument, during the whole period between May 05 and May 30 ($O_3 - O_3^q$). Top right panel: Temperature profiles expressed in K. Bottom right panel: same for temperature Relative difference profiles of the temperature expressed in [%]. Quiet conditions correspond to the period spanning from May 5 to May 9, 2024. The vertical black line displays the day when the daily Dst index reached its minimal value proton flux observed by GOES increased on May 10th, indicating the end-beginning of the main phase of the geomagnetic storm SPE that peaked on May 11 also corresponding to the peak proton flux for the event 11th.

this region can lead to large values of the relative difference. Moreover, after the event until May 17th, the loss in of ozone was observed in the tertiary layer between 70 km and 80 km. At those altitudes however, only around 75 km, in the tertiary layer, the decrease in ozone vmr was about 30%. At 70 km, 20% of the ozone is depleted from the mesosphere after the storm. This ozone decrease is only observed down to 70 km and until May 18th. In addition to the mesospheric ozone loss, in the MLT region above 90 km, a smaller depletion is observed by MLS. As for the lower altitudes

On the contrary, two days before the peak of the storm, the ozone vmr in the secondary layer did increase around 85 km. This is visible in the detrended time series of Fig. 4 and in the first panel of Fig. 5 in which the secondary layer slightly expanded. The largest increase was observed at 84 km of altitude, corresponding to the lower edge of the layer. This results in the positive values of the relative difference profiles observed at this altitude in the bottom panel of the figure.

Nonetheless, the slightly expanded layer was also impacted by the storm. Similar to the tertiary layer, the decrease of ozone vmr in the MLT seems to start above 80 km started one day before the peak of the storm. However, the ozone loss is relatively small, mainly remaining below 10%. Nonetheless, the ozone depletion reached 20% and 15% on May 13th and 17th respectively corresponding to periods of increased electron precipitation (see Fig. 2 bottom panel). Finally, no significant change in $O_3 - O_3^q$ vmr has been observed by MLS after the storm of May in the stratosphere.

The bottom-panel-right panels of Fig. 5 is are the same as the top-panel-left panels, but for the temperature measurements from MLS. The observations of the absolute temperature (top right) show a warming of the atmosphere

above 70 km starting on May 10 while a clear decrease of temperature can be observed starting on May 16th between 60 km and 50 km. The changes observed during this period are confined between -5% and 5% through the entire altitude range. However, it is apparent in the figure that after the storm and SEP-SPE of May 11th, the entire atmosphere above 75 km heats up while below this altitude, the general trend is a cooling, except from May 27th to the 31th between 45 km and 70 km. It is important to note that the warming of the upper atmosphere starts two days before the event. As for the ozone, this premature atmospheric warming coincides with the early arrival of low energy protons in the atmosphere, as well as an early increase of electron precipitation before the SEP-SPE took place. Below 40 km, the temperature constantly decreases from the event onward. However, this change in temperature is mainly caused by the seasonal variability. The heating observed in the upper part of the atmosphere is most likely caused by particle heating and joule heating. A part of the energy of the EPP is lost as heat in the atmosphere and some of its energy is dissipated when they move in the effective electric field of the Earth (Sinnhuber et al. (2012)).

3.6 Observations of ozone and temperature in June

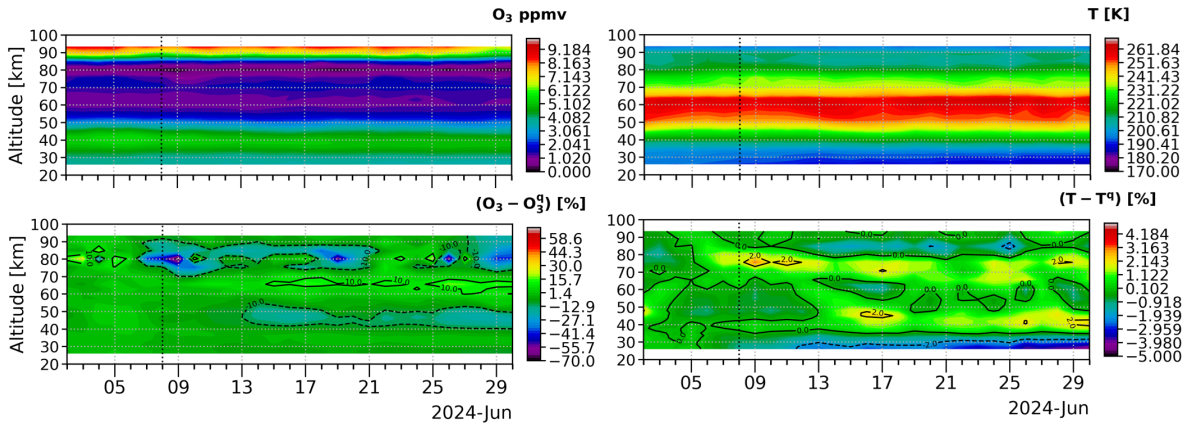


Figure 6. Top left panel: Absolute values of the O_3 vmr measured by the AURA/MLS instrument in the southern hemisphere throughout the month of June 2024. Bottom left panel: Relative difference (in [%]) between the mean quiet condition ozone profiles (O_3^q) and the daily ozone profiles (O_3) from the AURA/MLS instrument, during the whole period between June 02-2 and June 30 (03)30. Top right panel: Temperature profiles expressed in K. Bottom right panel: same for temperature Relative difference profiles of the temperature expressed in [%]. Quiet conditions correspond to the period spanning from June 02-2 to June 07-7, 2024. The vertical black line displays the day of peak proton flux for this event.

The two-four panels of Fig. 6 are similar to those of Fig. 5 but for MLS observations just before and after the SEP-SPE of June 8th. Again, the top-panel-shows-left panels show the results for ozone. Despite being more intense than in May, this SEP-SPE also had no influence on the stratospheric ozone. At around 50 km, the ozone vmr gradually decreases from the time of the SEP-SPE onward. Below this altitude, no noticeable change was observed by MLS. The slow ozone depletion MLS instrument

285 did not observe noticeable change. The decrease in ozone at 50 km that starts one day before the SPE, which remains until the
end of June, can be explained by long-term long-term (seasonal) variations rather than combined with the effect of EPP (see
 Fig. 1 middle panel). The day following the proton injection of June, AURA/MLS measurements show a depletion of 60% in
 ozone vmr at 80 km. Although not as intense as at 80 km, the depletion in $\Theta_3\text{-O}_3$ vmr occurred between 70 km and 90 km and
 was of about approximately 20%. In the MLT region, no change in ozone is discernible in the observations.

The bottom panel right panels of the figure shows the relative difference in atmospheric show the results for the temperature.
 290 The maximum changes in temperature observed in June are limited between -2% and 2%, which is quite less that than in May.
 As in May, below 40 km, the temperature observations show a steady decrease caused by seasonal variations as winter starts
 in the SH. Between 40 km and 80 km, the general behavior of the atmosphere is a small warming which is lasting for remains
during the whole period as is, not likely to be linked to the proton precipitation particle precipitation.

3.7 Comparison with previous years

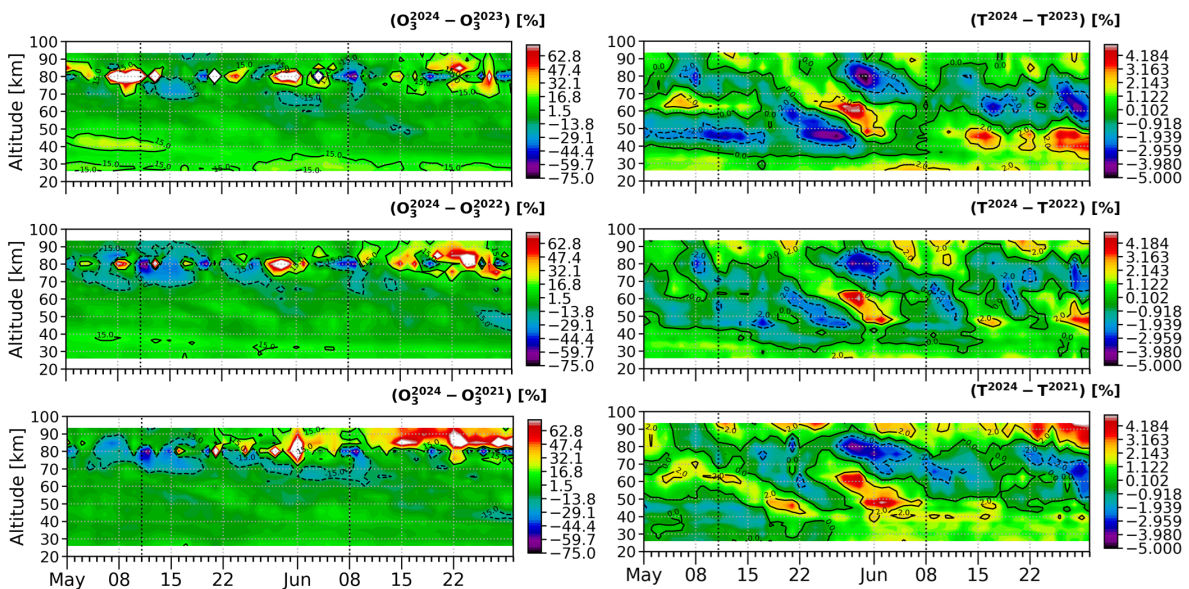


Figure 7. Comparison between the daily averaged ozone profiles (left) and temperature profiles (right) in the southern polar hemisphere
from 1 May to 30 June. From top to bottom, each panel corresponds to the relative difference in % between 2024 and 2023, 2022 and 2021
respectively. The vertical dotted lines in each panel corresponds to the peak flux of the May and June SPE.

295 Figure 7 shows the results of the comparison between the daily averaged observations performed by the MLS instrument
between May 1st and June 30th 2024 and the daily averaged observations from the three previous years at the same period.
These years and more specifically this period for each year (2023, 2022 and 2021) constitute a good basis to assess if the
changes in ozone and temperature observed in 2024 are caused by the particle forcing. In 2021 and 2022, between May and

300 June, no SPE was observed by GOES and only one moderate geomagnetic storm occurred. This period in 2023 was more active than for the two previous years. One SPE associated to a moderated geomagnetic storm took place on May 8th. Following this event, MLS observations showed a decrease of 15% in the amount of ozone between 70 km and 80 km for 3 days. This can be seen in the upper left panel of the figure as the ozone measurements in 2024 are more that 15% higher than in 2023 between May 8th and May 11th.

305 In all panels of Fig. 7, the ozone measurements in 2024 are lower by at least 15% than the three previous years following May 11th and June 8th between 70 km and 80 km. Compared to 2020 and 2023, the ozone vmr in 2024 was also lower a few days before the SPE took place. However, just after the event, the difference is more significant (up to 50%). Following the event on June, ozone vmr measured in 2024 are also always smaller than for the 3 previous years between 70 km and 80 km.

310 At altitudes below 60 km, the left panels of the figure show that the ozone vmr is generally higher in 2024 than in 2023 and 2022. However, no change in the relative difference occurs after neither the May nor the June events. At altitudes above 80 km, the ozone vmr measured in 2024 is lower after the May event than in 2023 (by 10%), 2022 (by 15%). This is not the case for the June event.

315 The right panels of Fig. 7 display the comparison between the daily average temperatures in 2024 and the 3 previous years. The significant heating that occurs after the event of May 11th 2024 above 80 km is clearly visible in all panels of the figure. Following the storm of May, the temperature at those altitudes in 2024 is always higher than at the same period for the previous years. The largest difference is observed with the measurements of 2021 while the smallest difference is observed with the measurements of 2023. For the event of June, despite the fact that the temperature was slightly cooling after the SPE above 80 km, the comparison of the observations with those of the previous years shows that the temperature in 2024 remains the highest of all the periods considered. In this comparison again, no significant changes in the temperature are observed before and after the storm.

320 The same figures were made for the observations of the MLS instrument in the northern hemisphere (not shown here) and no significant impact of either events could be observed. Only after the SPE and the extreme geomagnetic storm of May, a 15% ozone decrease above 70 km was seen relative to the quiet conditions. However, even before the precipitation of particles in the atmosphere, ozone vmr at those altitudes showed similar variability. The comparison of the observations in 2024 with the observations of the 3 previous years confirmed that the decrease following the event of May in the northern hemisphere is difficult to differentiate from other random variability.

4 Discussion and conclusions

In this work, we presented the first observations of the atmospheric ozone response to the extreme geomagnetic storm and **SEP SPEs** that took place on May 11th and June 8th 2024. We mainly used AURA/MLS observations which provided measurements of ozone and temperature profiles at high latitude in both hemispheres ~~due to its low Earth orbit~~. Moreover, computations of the ionization rate for both events were performed with the AtRIS toolkit combined with the observations from GOES.

330 These observations allowed us to demonstrate that:

- Following the May and June SPE, substantial ozone destruction was measured during several days in the southern polar hemisphere at altitudes between 70-80 km. Comparison with the observations at the same period but for previous years supports the fact the ozone variations in 2024 are caused by the particle precipitations.
- 335 – The ozone depletion in this altitude range lasted longer after the events of May (5 days) than in June (3 days). This difference in the ozone response can be explained by the ionization rates produced by the SPEs, which were generally higher in May than in June. Moreover, the SPE of May 11th was accompanied by the most extreme geomagnetic storm seen in 20 years that caused a large precipitation of energetic electrons in the atmosphere.
- Despite the fact that both June and May SPEs led to an increase in the ionization rate down to 35 km, observations of
340 the MLS instrument show no signs of a decrease in ozone concentration in the upper stratosphere.

The responses of ozone and temperature to the ~~event events~~ of May 11th and June 8th are quite different. For ozone, this can be seen in both the detrended ozone time series in Fig. 4, as well as in the relative difference profiles shown in Fig. 5 and Fig. 6. Much stronger and ~~longer-lasting-longer-lasting~~ ozone depletion is observed through the atmosphere in May than in June. However, this is ~~easily~~-explained by the difference in the flux of EPP during the two events. In May, an overlap between
345 energetic solar protons observed by GOES and strongly enhanced electron fluxes from the radiation belts observed by POES have precipitated in the atmosphere. ~~In~~, while in June, electron precipitation ~~is was~~ observed the day before the ~~SEP-SPE~~ reached the Earth, but ~~does did~~ not continue due to the lack of strong geomagnetic disturbances for this event. The computation with AtRIS of those two SPEs also shows that after the first and most energetic proton peak flux of each event, the ionization rate (caused by the second proton peak flux) in May is increased significantly more in May (~ 10 [pair/(s cm³)] than in June
350 (~ 1 [pair/(s cm³)] and lasting for ~ 8 days compared to ~ 5 days in June.

~~Aside the seasonal variations, there is a clear difference in the behavior of ozone in the northern and southern hemisphere after the precipitation of energetic particles in the high-latitude atmosphere. During the event of May 11th, MLS observations show a clear decrease of ozone in the southern polar mesosphere. In the northern hemisphere however, only two short-lived decreases in ozone took place in the MLT region above 90 km, on May 13th and on the 17th, each of them lasting~~
355 ~~for two days. These inter-hemispheric differences are strongly linked to the local season. For geomagnetic activity, hence electron precipitation, Mironova et al. (2023) showed through a one-dimensional Radiative-Convective-Photochemical model that ozone depletion in the mesosphere was only possible during local spring, winter and fall, with the strongest one only taking place in winter. Those conclusions also apply for solar protons as shown with MLS observations between 2004 and 2024 by Doronin et al. (2024) and by Xiong et al. (2023) for the severe SEP of January 2012. In our observations of the June SEP, no~~
360 ~~significant changes in O_3 were observed in the northern hemisphere whereas a drop of 60% occurred at~~ For the temperature, after the extreme storm of May, measurements of the MLS instrument show a warming of the atmosphere above 80 km. This is in agreement with the recent study from Liu et al. (2025) in which they report a global increase in the temperature of the MLT region during this event with observations performed by the SABER instrument. Conversely, in June, we observe a 2% cooling of the atmosphere above 80 km ~~in the polar-southern hemisphere.~~

365 ~~In the MLT region while the atmosphere between 70 and 80 km heats up by 2%. In the secondary layer,~~ decreases in ozone
are only observed ~~during the event following the SPE of May 2024. At those altitudes, the maximum decrease in O_3 is reached~~
~~two~~ Above 80 km, the detrended ozone time series show a decrease in ozone starting on the day of the event (this is also
observed at 84 km, where the ozone vmr suddenly increased the day before the SPE). A 10% depletion in O_3 is reached five
days after the storm unlike in the mesosphere where it is reached in one day. ~~In the MLT region, Jia et al. (2024) have discussed~~
370 ~~that the~~ Those changes in ozone at those altitudes could be related to the increase of the temperature that followed the event
(Jia et al. (2024)). Comparison with observations from the previous years shows that the increase of the temperature above 80
km and the decrease in ozone ~~are not linked to catalytic reactions with HO_x and NO_x , but rather to changes in~~ above 85
km are unique features of the year 2024 and that they arise after the event of May. However, due to the complexity of the
dynamics in this region of the atmosphere, the measurements of the MLS instrument alone are not sufficient to determine the
375 physical processes that led those changes. Further investigations with a model of the MLT region are required to draw educated
conclusions.

On May 11th, during the main phase of the extreme geomagnetic storm, the ~~mean meridional circulation (MMC) induced by~~
~~EPP. The perturbed MMC transports $[O]$ and $[H]$ in the polar MLT which, associated to the heating of the thermosphere, can~~
~~lead to the decrease of~~ peak of solar protons fluxes and thus the largest increase in atmospheric ionization rates, observations
380 of the MLS instrument show a clear drop in the amounts of ozone in the southern polar mesosphere. The detrended time series
shown in Fig. 4 also indicate that the ozone concentration. This process may explain the changes of ozone observed after the
in the secondary and tertiary layers decreased simultaneously during the storm of May which featured a significant heating of
the upper atmosphere. Furthermore, in June, no significant heating of the lower thermosphere was observed by MLS and no
significant variation of ozone is observed. However, observations of $[O]$ and $[H]$ should be considered to verify this hypothesis.

385 Finally, measurements from MLS do not show a quick response of stratospheric ozone after the May and June events. In
both cases, the spectrum of solar protons was hard enough to produce ionization in the upper stratosphere. In May, which is
in agreement with the relative difference profiles presented in Fig. 5. However, the detrended time series show that the largest
variations in absolute values occurred in the MLT whereas the largest variations observed in the relative differences are observed
390 in the tertiary layer. This is explained by the fact that the absolute values of ozone are lower (around 1.5 ppmv) compared to
the secondary layer in which the absolute values of ozone vmr are higher (around 8.5 ppmv). Between 70 km and 80 km,
ozone was depleted until May 17th, which corresponds to the period of time in which the ionization rates are significantly
increased at those altitudes (see Fig. 3). Subsequently, the depletion in ozone persists but only between 75 km and 80 km until
May 27th. In June, the injection of solar protons in the atmosphere also led to a significant increase of the ionization rate. The
395 most significant increase occurred on June 8th between 70 km and 90 km and lasted for 2 days. During this period, a depletion
of ozone of at least 20% was observed at the same altitudes and lasting for 3 days. The comparison of the observations from
2024 and the three previous years (2023, 2022, 2021) confirmed that the ozone depletion that followed both SPEs between 70
km and 80 km were most likely caused by the increase of the ionization rates induced by solar protons. In both cases, ozone
levels in this altitude range were consistently lower in 2024 than during the same period in previous years. Again in June, no

400 significant ~~change in ozone concentrations is observed below 60 km. This absence of response in stratospheric ozone could be explained by the season again. Indeed, Denton et al. (2018) have shown in the northern hemisphere with observations of 191 SEPs that ozone depletion following an event was never observed in absence of the polar vortex. Thus, stratospheric depletions are only visible during polar winter, which is not the case in May in the southern hemisphere. In June, ozone is depleted by 10% 5 days after the storm. However, this slow decrease~~ changes in ozone were observed following the event in the northern
405 mesosphere. At higher altitudes, in the lower thermosphere no variation of ozone over time is fitting the long-term variation of ozone computed with the lowess algorithm was observed following the SPE.

In addition to seasonal variations, there is a clear difference in the behavior of ozone in the northern and southern hemisphere after the precipitation of energetic particles in the high-latitude atmosphere. Following the event of May 11th, in the northern hemisphere, ozone observed by AURA/MLS in the MLT decreased by 15%. Pierrard et al. (2025a) have also shown a decrease
410 of total ozone content in the northern hemisphere on 10 and 11 May 2024 associated to a peak of ultraviolet radiation. The interhemispheric differences in the response of ozone are strongly linked to the local season, when the amount of sunlight at polar latitudes greatly differs between local winter/summer. This difference in sunlight is partly responsible for the difference in the quiet-time composition of the mesosphere by influencing the ozone concentration (Smith et al. (2018a)) and the ozone depleting species like HO_x (Chen (2022)) and NO_x. Moreover, even though June marks the winter in the SH, the decrease in
415 ozone concentration observed by MLS is not consistent with a descent of NO_x from high altitudes, as no depletion is observed between 60 km and 70 km. In addition, a direct production of NO_x in the upper stratosphere would cause a decrease of ozone quickly after the storm, which is not observed here. difference in illumination in the two polar hemispheres leads to a different evolution of NO_x species following their production by the particles injected during the storm. For the intense SPE of January 2012, Xiong et al. (2023) showed that the larger amount of HO_x present in the summer than in the winter during quiet
420 time led to smaller increase of HO_x during the SPE in the summer hemisphere than in the winter hemisphere, thus changing the ozone response to the event. For NO_x species, the increased concentrations caused by the storm evolve differently under different lighting conditions. In the winter hemisphere, HO_x is long-lived whereas in the summer hemisphere, it is depleted by photodissociation and photoionization. In turn, the response of ozone to the particle precipitation is different in the two hemispheres.

425 Finally, although both SPEs increased ionization down to 30 km (up to 30 pairs/(s·cm³)), no change in ozone concentration was observed in the stratosphere between 30 km and 60 km following these events. However, those two SPEs are not unusually large compared to previous events. Studies that demonstrated a decrease of upper stratospheric ozone driven by a SPE showed that the ionization rate between 30 km and 60 km was significantly higher (up to 10000 [pair/(s·cm³)] in 2003 in Funke et al. (2011)) than what we computed for May and June 2024.

430 *Data availability.* All data are available in the zenodo (Winant et al. (2024)). OMNI data are available at <https://omniweb.gsfc.nasa.gov/ow.html>, Version 5 of AURA/MLS level 2 data and user recommendations can be found at <https://disc.gsfc.nasa.gov/datasets>, GOES proton inte-

gral fluxes can be found at GOESdataareaccessibleat:<https://lasp.colorado.edu/space-weather-portal/>, MEPED electron fluxes are accessible at [tps://lasp.colorado.edu/space-weather-portal/](https://lasp.colorado.edu/space-weather-portal/)

435 *Author contributions.* AW made the present analyses and wrote the manuscript with the contribution of the other authors. VP conceptualized and supervised the study, and contributed to the interpretation of the results. All authors contributed to writing of the manuscript through reviews and edits.

Competing interests. The author declare that they have no conflict of interests

440 *Acknowledgements.* The project 21GRD02 BIOSPHERE has received funding from the European Partnership on Metrology, co-financed by the European Union's Horizon Europe Research and Innovation Programme and by the Participating States. The authors acknowledge the Horizon 2020 PITHIA-NRF project with Grant Agreement 101007599.

The results presented in this document rely on data provided by the Community Coordinated Modeling Center at Goddard Space Flight Center through their integrated Space Weather Analysis (iSWA) system's HAPI server (<https://iswa.gsfc.nasa.gov/IswaSystemWebApp/hapi>). The CCMC is a multi-agency partnership between NASA, AFMC, AFOSR, AFRL, AFWA, NOAA, NSF and ONR. These data were accessed via the University of Colorado's Space Weather Technology, Research, and Education Center's (<https://colorado.edu/spaceweather>)
445 Space Weather Data Portal (<https://lasp.colorado.edu/space-weather-portal>).

References

- Abe, O., Fakomiti, M., Igboama, W., Akinola, O., Ogunmodimu, O., and Migoya-Orué, Y.: Statistical analysis of the occurrence rate of geomagnetic storms during solar cycles 20–24, *Advances in Space Research*, 71, 2240–2251, 2023.
- Andersson, M. E., Verronen, P. T., Wang, S., Rodger, C. J., Clilverd, M. A., and Carson, B. R.: Precipitating radiation belt electrons and
450 enhancements of mesospheric hydroxyl during 2004–2009, *Journal of Geophysical Research: Atmospheres*, 117, 2012.
- Andersson, M. E., Verronen, P. T., Rodger, C. J., Clilverd, M. A., and Seppälä, A.: Missing driver in the Sun–Earth connection from energetic electron precipitation impacts mesospheric ozone, *Nature Communications*, 5, 5197, <https://doi.org/10.1038/ncomms6197>, 2014.
- Banjac, S., Herbst, K., and Heber, B.: The atmospheric radiation interaction simulator (atris): Description and validation, *Journal of Geophysical Research: Space Physics*, 124, 50–67, 2019.
- 455 Chen, Z.: First observations of mesospheric OH emission profiles from OMPS/LP, *Journal of the Atmospheric Sciences*, 79, 1057–1067, 2022.
- Cleveland, W. S.: Robust locally weighted regression and smoothing scatterplots, *Journal of the American statistical association*, 74, 829–836, 1979.
- Denton, M. H., Kivi, R., Ulich, T., Clilverd, M. A., Rodger, C. J., and von der Gathen, P.: Northern hemisphere stratospheric ozone depletion
460 caused by solar proton events: the role of the polar vortex, *Geophysical Research Letters*, 45, 2115–2124, 2018.
- Doronin, G., Mironova, I., Bobrov, N., and Rozanov, E.: Mesospheric Ozone Depletion during 2004–2024 as a Function of Solar Proton Events Intensity, *Atmosphere*, 15, 944, 2024.
- Ellison, D. C. and Ramaty, R.: Shock acceleration of electrons and ions in solar flares, *Astrophysical Journal, Part 1 (ISSN 0004-637X)*, vol. 298, Nov. 1, 1985, p. 400-408. NASA-supported research., 298, 400–408, 1985.
- 465 Elvidge, S. and Themens, D. R.: The probability of the May 2024 geomagnetic superstorm, *Space Weather*, 23, e2024SW004 113, 2025.
- Evans, D. and Greer, M.: Polar orbiting environmental satellite space environment monitor, NOAA National Geophysical Data Center, 2000.
- Evans, J. S., Correira, J., Lumpe, J. D., Eastes, R. W., Gan, Q., Laskar, F. I., Aryal, S., Wang, W., Burns, A. G., Beland, S., Cai, X., Codrescu, M., England, S., Greer, K., Krywonos, A., McClintock, W. E., Plummer, T., and Veibell, V.: GOLD Observations of the Thermospheric Response to the 10–12 May 2024 Gannon Superstorm, *Geophysical Research Letters*, 51, e2024GL110506,
470 <https://doi.org/10.1029/2024GL110506>, 2024.
- Funke, B., López-Puertas, M., Gil-López, S., Von Clarman, T., Stiller, G. P., Fischer, H., and Kellmann, S.: Downward transport of upper atmospheric NO_x into the polar stratosphere and lower mesosphere during the Antarctic 2003 and Arctic 2002/2003 winters, *Journal of Geophysical Research: Atmospheres*, 110, 2005JD006 463, <https://doi.org/10.1029/2005JD006463>, 2005.
- Funke, B., Baumgaertner, A., Calisto, M., Egorova, T., Jackman, C. H., Kieser, J., Krivolutsky, A., López-Puertas, M., Marsh, D. R., Reddmann, T., et al.: Composition changes after the " Halloween " solar proton event: the High Energy Particle Precipitation in the Atmosphere (HEPPA) model versus MIPAS data intercomparison study, *Atmospheric Chemistry and Physics*, 11, 9089–9139, 2011.
- 475 Funke, B., López-Puertas, M., Stiller, G., and Von Clarman, T.: Mesospheric and stratospheric NO_y produced by energetic particle precipitation during 2002–2012, *Journal of Geophysical Research: Atmospheres*, 119, 4429–4446, 2014.
- Funke, B., López-Puertas, M., Stiller, G. P., Versick, S., and von Clarman, T.: A semi-empirical model for mesospheric and stratospheric
480 NO_y produced by energetic particle precipitation, *Atmospheric Chemistry and Physics*, 16, 8667–8693, 2016.
- Grenfell, J. L., Lehmann, R., Mieth, P., Langematz, U., and Steil, B.: Chemical reaction pathways affecting stratospheric and mesospheric ozone, *Journal of Geophysical Research: Atmospheres*, 111, 2004JD005 713, <https://doi.org/10.1029/2004JD005713>, 2006.

- Hayakawa, H., Ebihara, Y., Mishev, A., Koldobskiy, S., Kusano, K., Bechet, S., Yashiro, S., Iwai, K., Shinbori, A., Mursula, K., et al.: The Solar and Geomagnetic Storms in 2024 May: A Flash Data Report, *The Astrophysical Journal*, 979, 49, 2025.
- 485 Herbst, K., Muscheler, R., and Heber, B.: The new local interstellar spectra and their influence on the production rates of the cosmogenic radionuclides ^{10}Be and ^{14}C , *Journal of Geophysical Research: Space Physics*, 122, 23–34, 2017.
- Huang, F., Lei, J., Zhang, S.-R., Wang, Y., Li, Z., Zhong, J., Yan, R., Aa, E., Zhima, Z., and Luan, X.: Peculiar nighttime ionospheric enhancements over the Asian sector during the May 2024 Superstorm, *Journal of Geophysical Research: Space Physics*, 129, e2024JA033 350, 2024.
- 490 Jackman, C. H., McPeters, R. D., Labow, G. J., Fleming, E. L., Praderas, C. J., and Russell, J. M.: Northern hemisphere atmospheric effects due to the July 2000 Solar Proton Event, *Geophysical Research Letters*, 28, 2883–2886, <https://doi.org/10.1029/2001GL013221>, 2001.
- Jaswal, P., Sinha, S., and Nandy, D.: Deconstructing the Properties of Solar Super Active Region 13664 in the Context of the Historic Geomagnetic Storm of 2024 May 10–11, *The Astrophysical Journal*, 979, 31, 2025.
- Jia, J., Kero, A., Kalakoski, N., Szeląg, M. E., and Verronen, P. T.: Is there a direct solar proton impact on lower-stratospheric ozone?,
 495 *Atmospheric Chemistry and Physics*, 20, 14 969–14 982, 2020.
- Jia, J., Murberg, L. E., Løvset, T., Orsolini, Y. J., Espy, P. J., Zeller, L. C., Salinas, C. C. J. H., Lee, J. N., Wu, D., and Zhang, J.: Energetic particle precipitation influences global secondary ozone distribution, *Communications Earth & Environment*, 5, 270, 2024.
- Kwak, Y.-S., Kim, J.-H., Kim, S., Miyashita, Y., Yang, T., Park, S.-H., Lim, E.-K., Jung, J., Kam, H., Lee, J., et al.: Observational Overview of the May 2024 G5-Level Geomagnetic Storm: From Solar Eruptions to Terrestrial Consequences, *Journal of Astronomy and Space*
 500 *Sciences*, 41, 171–194, 2024.
- Lary, D.: Catalytic destruction of stratospheric ozone, *Journal of Geophysical Research: Atmospheres*, 102, 21 515–21 526, 1997.
- Liu, X., Xu, J., Yue, J., Wang, W., and Moro, J.: Mesosphere and Lower Thermosphere Temperature Responses to the May 2024 Mother’s Day Storm, *Geophysical Research Letters*, 52, e2024GL112 179, <https://doi.org/10.1029/2024GL112179>, 2025.
- Marsh, D., Smith, A., Brasseur, G., Kaufmann, M., and Grossmann, K.: The existence of a tertiary ozone maximum in the high-latitude
 505 middle mesosphere, *Geophysical Research Letters*, 28, 4531–4534, 2001.
- Mavromichalaki, H., Papailioui, M.-C., Livada, M., Gerontidou, M., Paschalis, P., Stassinakis, A., Abunina, M., Shlyk, N., Abunin, A., Belov, A., et al.: Unusual Forbush Decreases and Geomagnetic Storms on 24 March, 2024 and 11 May, 2024, *Atmosphere*, 15, 1033, 2024.
- Mironova, I., Aplin, K. L., Arnold, F., Bazilevskaya, G. A., Harrison, R. G., Krivolutsky, A. A., Nicoll, K. A., Rozanov, E. V., Turunen, E., and Usoskin, I. G.: Energetic particle influence on the Earth’s atmosphere, *Space science reviews*, 194, 1–96, 2015.
- 510 Mironova, I., Grankin, D., and Rozanov, E.: Mesospheric ozone depletion depending on different levels of geomagnetic disturbances and seasons, *Atmosphere*, 14, 1205, 2023.
- Pesnell, W. D. and Schatten, K. H.: An early prediction of the amplitude of solar cycle 25, *Solar Physics*, 293, 112, 2018.
- Pickett, H. M., Read, W. G., Lee, K. K., and Yung, Y. L.: Observation of night OH in the mesosphere, *Geophysical Research Letters*, 33, 2006GL026 910, <https://doi.org/10.1029/2006GL026910>, 2006.
- 515 Pierrard, V., Winant, A., Botek, E., and Péters de Bonhome, M.: The Mother’s Day Solar Storm of 11 May 2024 and Its Effect on Earth’s Radiation Belts, *Universe*, 10, 391, 2024.
- Pierrard, V., Bolsee, D., et al.: BIOSPHERE measurement campaign from January 2024 to March 2024 and in May 2024: Effects of the solar events on the radiation belts, UV radiation and ozone in the atmosphere, *Geoscience*, 11, 17–154, 2025a.
- Pierrard, V., Verhulst, T., Chevalier, J.-M., Bergeot, N., and Winant, A.: Effects of the Geomagnetic Superstorms of 10–11 May 2024 and
 520 7–11 October 2024 on the Ionosphere and Plasmasphere, *Atmosphere*, 6, 299, 2025b.

- Randall, C., Harvey, V., Singleton, C., Bailey, S., Bernath, P., Codrescu, M., Nakajima, H., and Russell III, J.: Energetic particle precipitation effects on the Southern Hemisphere stratosphere in 1992–2005, *Journal of Geophysical Research: Atmospheres*, 112, 2007.
- Ranjan, A. K., Nailwal, D., Sunil Krishna, M. V., Kumar, A., and Sarkhel, S.: Evidence of Potential Thermospheric Overcooling During the May 2024 Geomagnetic Superstorm, *Journal of Geophysical Research: Space Physics*, 129, e2024JA033148, <https://doi.org/10.1029/2024JA033148>, 2024.
- 525 Rodger, C. J., Clilverd, M. A., Green, J. C., and Lam, M. M.: Use of POES SEM-2 observations to examine radiation belt dynamics and energetic electron precipitation into the atmosphere, *Journal of Geophysical Research: Space Physics*, 115, 2010.
- Rozanov, E., Calisto, M., Egorova, T., Peter, T., and Schmutz, W.: Influence of the precipitating energetic particles on atmospheric chemistry and climate, *Surveys in geophysics*, 33, 483–501, 2012.
- 530 Sætre, C., Stadsnes, J., Nesse, H., Aksnes, A., Petrinec, S., Barth, C., Baker, D., Vondrak, R., and Østgaard, N.: Energetic electron precipitation and the NO abundance in the upper atmosphere: A direct comparison during a geomagnetic storm, *Journal of Geophysical Research: Space Physics*, 109, 2004.
- Sátori, G., Williams, E., Price, C., Boldi, R., Koloskov, A., Yampolski, Y., Guha, A., and Barta, V.: Effects of energetic solar emissions on the Earth–ionosphere cavity of Schumann resonances, *Surveys in Geophysics*, 37, 757–789, 2016.
- 535 Schwartz, M.: MLS/Aura Level 2 Ozone (O3) Mixing Ratio V005, <https://doi.org/10.5067/AURA/MLS/DATA2516>, 2021.
- Seppälä, A., Matthes, K., Randall, C., and Mironova, I.: What is the solar influence on climate? Overview of activities during CAWSES-II. *Progress in Earth and Planetary Science*, 1, 24, DOI. ADS, 2014.
- Seppälä, A., Verronen, P. T., Sofieva, V. F., Tamminen, J., Kyrölä, E., Rodger, C. J., and Clilverd, M. A.: Destruction of the tertiary ozone maximum during a solar proton event, *Geophysical Research Letters*, 33, 2005GL025571, <https://doi.org/10.1029/2005GL025571>, 2006.
- 540 Singh, R., Scipión, D. E., Kuyeng, K., Condor, P., De La Jara, C., Velasquez, J. P., Flores, R., and Ivan, E.: Ionospheric disturbances observed over the Peruvian sector during the Mother’s Day Storm (G5-level) on 10–12 May 2024, *Journal of Geophysical Research: Space Physics*, 129, e2024JA033003, 2024.
- Sinnhuber, M., Nieder, H., and Wieters, N.: Energetic particle precipitation and the chemistry of the mesosphere/lower thermosphere, *Surveys in Geophysics*, 33, 1281–1334, 2012.
- 545 Smith, A. K. and Marsh, D. R.: Processes that account for the ozone maximum at the mesopause, *Journal of Geophysical Research: Atmospheres*, 110, 2005.
- Smith, A. K., Espy, P. J., López-Puertas, M., and Tweedy, O. V.: Spatial and temporal structure of the tertiary ozone maximum in the polar winter mesosphere, *Journal of Geophysical Research: Atmospheres*, 123, 4373–4389, 2018a.
- Smith, A. K., Espy, P. J., López-Puertas, M., and Tweedy, O. V.: Spatial and Temporal Structure of the Tertiary Ozone Maximum in the Polar Winter Mesosphere, *Journal of Geophysical Research: Atmospheres*, 123, 4373–4389, <https://doi.org/10.1029/2017JD028030>, 2018b.
- 550 Sofieva, V. F., Kyrölä, E., Verronen, P. T., Seppälä, A., Tamminen, J., Marsh, D. R., Smith, A. K., Bertaux, J.-L., Hauchecorne, A., Dalaudier, F., Fussen, D., Vanhellemont, F., Fanton d’Andon, O., Barrot, G., Guirlet, M., Fehr, T., and Saavedra, L.: Spatio-temporal observations of the tertiary ozone maximum, *Atmospheric Chemistry and Physics*, 9, 4439–4445, <https://doi.org/10.5194/acp-9-4439-2009>, 2009.
- Solomon, S., Rusch, D., Gérard, J.-C., Reid, G., and Crutzen, P.: The effect of particle precipitation events on the neutral and ion chemistry of the middle atmosphere: II. Odd hydrogen, *Planetary and Space Science*, 29, 885–893, 1981.
- 555 Solomon, S., Crutzen, P. J., and Roble, R. G.: Photochemical coupling between the thermosphere and the lower atmosphere: 1. Odd nitrogen from 50 to 120 km, *Journal of Geophysical Research: Oceans*, 87, 7206–7220, <https://doi.org/10.1029/JC087iC09p07206>, 1982.

- Themens, D. R., Elvidge, S., McCaffrey, A., Jayachandran, P., Coster, A., Varney, R. H., Galkin, I., Goodwin, L. V., Watson, C., Maguire, S., et al.: The high latitude ionospheric response to the major May 2024 geomagnetic storm: A synoptic view, *Geophysical Research Letters*, 51, e2024GL111 677, 2024.
- 560
- Turunen, E., Verronen, P. T., Seppälä, A., Rodger, C. J., Clilverd, M. A., Tamminen, J., Enell, C.-F., and Ulich, T.: Impact of different energies of precipitating particles on NO_x generation in the middle and upper atmosphere during geomagnetic storms, *Journal of Atmospheric and Solar-Terrestrial Physics*, 71, 1176–1189, <https://doi.org/10.1016/j.jastp.2008.07.005>, 2009.
- Verronen, P. and Lehmann, R.: Analysis and parameterisation of ionic reactions affecting middle atmospheric HO_x and NO_y during solar proton events, in: *Annales Geophysicae*, vol. 31, pp. 909–956, Copernicus Publications Göttingen, Germany, 2013.
- 565
- Verronen, P., Rodger, C. J., Clilverd, M. A., and Wang, S.: First evidence of mesospheric hydroxyl response to electron precipitation from the radiation belts, *Journal of Geophysical Research: Atmospheres*, 116, 2011.
- Verronen, P. T., Seppälä, A., Kyrölä, E., Tamminen, J., Pickett, H. M., and Turunen, E.: Production of odd hydrogen in the mesosphere during the January 2005 solar proton event, *Geophysical Research Letters*, 33, 2006GL028 115, <https://doi.org/10.1029/2006GL028115>, 2006.
- 570
- Winant, A., Pierrard, V., Botek, E., and Herbst, K.: The atmospheric influence on cosmic-ray-induced ionization and absorbed dose rates, *Universe*, 9, 502, 2023.
- Winant, A., Pierrard, V., and Botek, E.: Ozone decrease observed in the upper atmosphere following the May 11th 2024 Mother’s day solar storm: dataset., <https://doi.org/10.5281/ZENODO.14388032>, 2024.
- Xiong, S., Li, J., Wei, G., Lu, J., Tian, Y., Zhang, X., Fu, S., Sun, M., Li, Z., Zhang, H., et al.: The northern and southern hemispheric asymmetries of mesospheric ozone at high latitudes during the January 2012 solar proton events, *Space Weather*, 21, e2023SW003 435, 2023.
- 575